

Simulation study of signal formation in position sensitive planar p-on-n silicon detectors after short range charge injection*

T. Peltola^{a,b,**}, V. Eremin^c, E. Verbitskaya^c, J. Härkönen^{d,b}

^a*Texas Tech University, Department of Physics and Astronomy, Lubbock, TX, 79409, USA*

^b*Helsinki Institute of Physics, P.O. Box 64 (Gustaf Hållströmin katu 2) FI-00014 University of Helsinki, Finland*

^c*Ioffe Institute, St. Petersburg 194021, Russian Federation*

^d*Ruder Bošković Institute, Zagreb, 10000, Croatia*

Abstract

Segmented silicon detectors (micropixel and microstrip) are the main type of detectors used in the inner trackers of Large Hadron Collider (LHC) experiments at CERN. Due to the high luminosity and eventual high fluence, detectors with fast response to fit the short shaping time of 20 ns and sufficient radiation hardness are required.

Measurements carried out at the Ioffe Institute have shown a reversal of the pulse polarity in the detector response to short-range charge injection. Since the measured negative signal is about 30-60% of the peak positive signal, the effect strongly reduces the CCE even in non-irradiated detectors. For further investigation of the phenomenon the measurements have been reproduced by TCAD simulations.

As for the measurements, the simulation study was applied for the p-on-n strip detectors similar in geometry to those developed for the ATLAS experiment and for the Ioffe Institute designed p-on-n strip detectors with each strip having a window in the metallization covering the p^+ implant, allowing the generation of electron-hole pairs under the strip implant. Red laser scans across the strips and the interstrip gap with varying laser diameters and Si-SiO₂ interface charge densities were carried out. The results verify the experimentally observed negative response along the scan in the interstrip gap. When the laser spot is positioned on the strip p^+ implant the negative response vanishes and the collected charge at the active strip proportionally increases.

The simulation results offer a further insight and understanding of the influence of the oxide charge density in the signal formation. The observed effects and details of the detector response for different charge injection

*Work performed in the framework of the CERN-RD50 collaboration.

**Corresponding author

Email address: timo.peltola@helsinki.fi (T. Peltola)

positions are discussed in the context of Ramo's theorem.

Keywords: Silicon radiation detectors; Strip sensors; Transient current; Charge collection; TCAD simulations

1. Introduction

Segmented silicon detectors, like micropixel and microstrip, are the primary detector types used in inner trackers of the Large Hadron Collider (LHC) experiments [1, 2, 3]. Due to the high luminosity and eventual high fluence, detectors with fast response to fit the short shaping time of 20 ns and sufficient radiation hardness are required. The detectors must operate in a high-radiation environment for at least 10 years, maintaining a sufficient performance regardless of the accumulating degradation of the silicon properties.

Detector development and tests include detailed studies of the current and charge response to give information on the carrier transport in the detector bulk and on the charge collection efficiency (CCE), thus to achieve guidelines of the detector operation after installation to the measurement set-up. Earlier studies of silicon strip detectors [4, 5, 6] have displayed a distinctive feature in the pulse response. The pulses of negative polarity have been observed from adjacent strips in the charge collection measurements, using either a collimated MeV proton beam with a range of few tens of microns, a pulse of light with an absorption length of several micrometers or alpha-particles. Since the value of the negative signal can be up to 60% of the positive one, the effect has a potential to strongly influence the interpretation of the charge collection results of irradiated detectors and therefore requires further clarification.

Due to their versatility and ability to reproduce not only generic behavior but also absolute values of measured silicon sensor characteristics before and after radiation, the Technology Computer-Aided Design (TCAD) numerical simulations have been applied as the next investigation tool in further studies of the aforementioned effect. The reliability and accuracy of the TCAD simulations have already been documented in several publications [7, 8, 9, 10, 11] and Ph.D. theses [12, 13].

TCAD simulations not only provide the numerical calculations of charge collection parameters like the electric field distribution, bulk silicon properties and radiation induced defects for strip detectors, but also allow to perform these calculations with respect to parameters like Si-SiO₂ interface charge density or laser diameter that would be next to impossible to realize experimentally. TCAD simulations are an invaluable tool in the study the electric fields inside a segmented detector, since these cannot be measured directly.

This paper presents TCAD simulation results on the investigation of the negative charge response of p-on-n Si microstrip detectors. An interpretation of the origin of the signal polarity and its dependencies related

to the Si-SiO₂ interface in the interstrip gap is provided.

The investigation of the experimentally observed absence of reversed polarity signals in infra-red laser, with a penetration depth of several hundred microns in silicon, illuminated strip sensors [5], as well as the possible sensitivity of n-on-p strip sensors to the effect are left to a follow-up study.

2. TCAD simulations set-up

All simulations in this paper were carried out using the Synopsys Sentaurus¹ finite-element Technology Computer-Aided Design (TCAD) software framework. In all modelled sensor structures the silicon bulk material was considered to have $\langle 100 \rangle$ crystal orientation.

For the simulation study of the observed charge collection behaviour in Refs. [5, 6] the 2-dimensional structures presented in figure 1 were applied. This was considered sufficient approach since, unlike for pixels, strip segmentation is monotonous along the second coordinate parallel to the sensor surface and provides no additional contribution to the local electric field evolution with voltage at the strip edges.

Both modelled strip sensor configurations, ATLAS and Ioffe Institute, had physical thicknesses set to 300 μm , while the pitches, strip widths and layer dimensions are given in table 1. Also the bulk dopings of the two sensor substrates were set equal $N_B = 1 \times 10^{12} \text{ cm}^{-3}$, that resulted in full depletion voltages well below 100 V. This was done to minimize any effect from the small discrepancies in thickness and resistivity in the real sensors (285 μm , 3–4 $\text{k}\Omega \cdot \text{cm}$ for the ATLAS and 300 μm , 5 $\text{k}\Omega \cdot \text{cm}$ for the Ioffe Institute design, respectively [5, 6]) and focus the simulation investigation to the differences in strip configurations. The peak concentrations of both backplane n^+ and strip p^+ implantations were $5 \times 10^{18} \text{ cm}^{-3}$ while both decayed to the bulk doping level within 1.0 μm depth using a gaussian profile. The area of the strip detectors used in measurements, $10 \times 10 \text{ mm}^2$, was taken into account by stretching the 2-dimensional structures to the third dimension by an area factor. As the earlier measurements showed the density of the interface states to be about $Q_f = 5 \cdot 10^{10} \text{ cm}^{-2}$ [6], this was used as the baseline for the study of the effect of varied Q_f at the Si-SiO₂ interface.

Both modelled sensors consisted of 3-strip structures, of which one strip close-ups are presented in figure 1. Illustrated in figure 1b is the Ioffe Institute design's window in metallization of the p^+ implant that allows the generation of electron-hole ($e-h$) pairs under the strip implant. As can be seen from figure 1, the

¹<http://www.synopsys.com>

Table 1: The layer dimensions and strip parameters for the two simulated sensor types. The $W_{\text{impl,Al}}$ are the widths of the strip implant and its metallization, respectively. The $t_{\text{Ox,Al}}$ are the oxide and aluminum layer thicknesses, respectively, while d_{impl} is the depth of the strip implantation.

Sensor type	Pitch [μm]	W_{impl} [μm]	W_{Al} [μm]	t_{Ox} [μm]	t_{Al} [μm]	d_{impl} [μm]
ATLAS	80.0	20.0	16.0	0.47	0.70	1.0
Ioffe Institute	100.0	40.0	10.0	0.47	0.70	1.0

metal overhangs of the strip implants in both sensor designs were set to $-2 \mu\text{m}$ to reduce the differences in strip metallizations to the Ioffe Institute design’s charge injection window.

In all designs each strip had a DC-coupled electrode at zero potential. The readout electrode was the centermost strip of the 3-strip sensor structure in all simulations. In the figures of section 3 it is always located at $x = 0 \mu\text{m}$. The reverse bias voltage was provided from the backplane contact.

To generate charge carriers in the detector, a red laser with a wavelength of 670 nm and penetration of about $7 \mu\text{m}$ in silicon, was applied. The pulse length was set to 1 ns to match the experimental value in Refs. [5, 6]. With intensity set to 20 W/cm^2 , this resulted in laser generated $e-h$ pair density of about $345 \mu\text{m}^{-2}$. Two laser spot diameters were used in the simulations, a $10 \mu\text{m}$ which was also the diameter applied in the measurement set-up [5, 6, 14] and a $1 \mu\text{m}$ to enable scanning beyond experimentally available resolution. The red laser allows the investigation of a transient signal generated separately by the drift of electrons or holes (depending on which side of the detector is being illuminated) [15]. All laser scans were carried out at room temperature ($T = 293 \text{ K}$).

3. Simulation results

The charge collection plots resulting from the red laser interstrip scans presented in this section, are always normalized to the maximum charge collected at the lowest value of Si-SiO₂ interface charge density Q_f in each figure. This is to provide straightforward comparison of varied values of Q_f and laser diameter for the given strip sensor configuration.

3.1. Interstrip scans with $10 \mu\text{m}$ diameter red laser

Simulation results for the cross strip scans of a strip detector with ATLAS design from the p^+ -strip side show that the collected charge correlates well with the topology of the strips and the $80 \mu\text{m}$ pitch is clearly

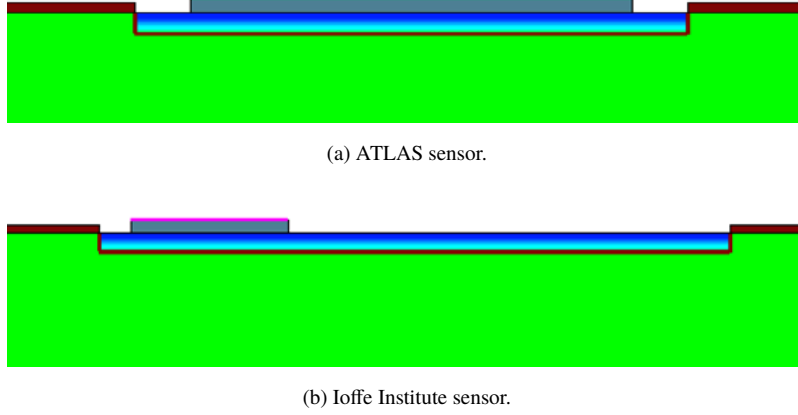


Figure 1: One strip close-up of the simulated 2-dim. 3-strip p-on-n sensor structures with parameters from table 1. Both (1a) ATLAS and (1b) Ioffe Institute "baby" strip detectors were $300\text{ }\mu\text{m}$ thick with a metal overhang of $-2\text{ }\mu\text{m}$. The Ioffe Institute detector has also a window in metallization for a charge injection from oxide-free region. The Al layers on top of the structures are illustrated in gray and the surrounding oxide layers are shown in brown. Strip implants are shown in blue while the green region is the lightly doped Si bulk. The n^+ layer and the metallization of the non-segmented backplane are not pictured.

recognizable, as can be seen from figure 2. When the laser position is either at the 'center implant', which is considered as the readout strip, or its adjacent strips, the resulting plots for the collected charge (Q_{coll}) contain low signal regions due to the opacity of the $16\text{ }\mu\text{m}$ wide metallization.

As in earlier measurements [5, 6], a significant reversed polarity signal is observed when the point of carrier injection is beyond midgap distance from the readout strip, i.e. when $|x| > 40\text{ }\mu\text{m}$ in figure 2. The negative signal at $|x| = 50\text{ }\mu\text{m}$ varies as a function of Q_f between 1% and 33% of the positive maximum, while the corresponding measured value was about 50% [5].

The charge collection scans display a strong dependence on interface charge density Q_f . When $x > \text{midgap}$ from the centermost strip in figure 2, the highest value of Q_f corresponds to the highest negative collected charge. However, the effect essentially vanishes at the lowest Q_f value of $1 \times 10^{10}\text{ cm}^{-2}$. When $x < \text{midgap}$, reversed behavior is observed, the highest Q_f now corresponds to the lowest positive collected charge until the implant edge is reached. The two highest value Q_f plots also present sensitivity to the strip implant edges. The electric field peaks at the implant edges react strongly to the increase of Q_f and start to amplify charges, both positive and negative, injected at their position. This is especially apparent for the highest Q_f value.

The corresponding red laser scan of a detector with Ioffe Institute design is presented in figure 3. The scan is now carried out across the strips with implant width of $40\text{ }\mu\text{m}$ but with metallization of only $10\text{ }\mu\text{m}$,

as presented in figure 1b. Scan results in the SiO_2 layer region and at the strip implants adjacent to the readout strip at the center show similar behavior to the ATLAS-design sensor results in figure 2, while the sharp drop of the signal from centermost strip now occurs only within the area of the metallization window of the p^+ implant.

As in earlier measurements [6], the maximum collected charges are observed in the area free from the metal contact at the centermost implant (x coordinates between -20 – $20 \mu\text{m}$). The amplitudes of the positive signals collected in the area of the oxide, with laser distance from the readout strip less than midgap, move from about 87% to 74% with increased values of Q_f . The amplitude of the negative signal at the region beyond the midgap from the collecting strip for different values of Q_f now varies between 13%–22% (as opposed to the measured 30%–40% [6]) of the maximal positive signal.

When the charge collection plots of equal Q_f values in figures 2 and 3 are compared, the two sensor designs display no significant differences at the strip implant edges. Thus, the doubled strip implant width, while maintaining equal interstrip gap size, of the Ioffe Institute-design sensor that results in lower average electric fields in the area of the strip implant for the given biasing voltages, presented in figure 4, has negligible effect on charge collection at the implant edge. Also the amplitudes of negative signals in the two figures match closely. Thus, the experimentally observed about 10% difference between the two sensor designs is not verified by simulation.

Overall the simulated red laser scans with diameter matching the experimental set-up reproduce reasonably well the measured charge collection behavior of the ATLAS- and Ioffe Institute-design strip detectors [5, 6].

3.2. Interstrip scans with $1 \mu\text{m}$ diameter red laser

For deeper understanding of the dependence of the collected charge on the interface states Q_f and the source of the reversed polarity or reduced signals, observed in section 3.1, the scans were next repeated with $1 \mu\text{m}$ diameter, 670 nm wavelength laser to achieve results with higher resolution.

The scan results for ATLAS-design strip detector in figure 5 are now significantly different to figure 2 and reveal new features of the charge collection behavior between strips. As displayed in figure 5 the charge collection of the highest Q_f value is amplified substantially at the implant edges due to small spatial spread of the laser that results in the charge injection to be focused at the position of the electric field maxima.

Also in figure 5 it can be seen that the polarity reversal of the signal at midgap takes place abruptly, within $5 \mu\text{m}$. When the laser spot is above the oxide the two highest values of Q_f are now collecting almost equal

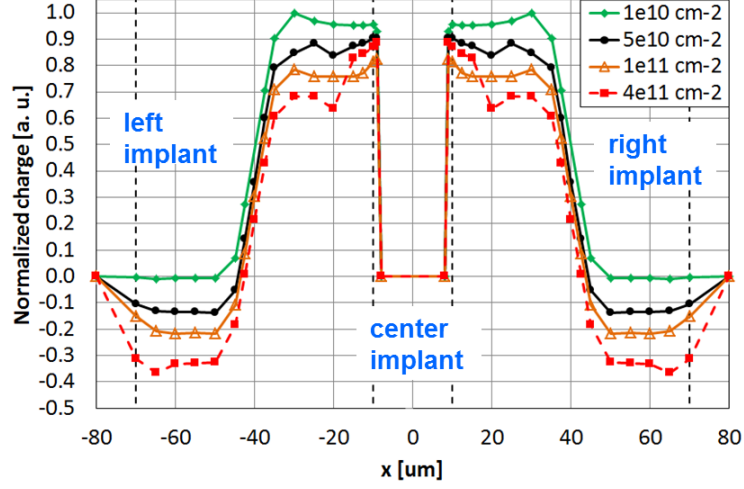


Figure 2: Charges collected at the centermost strip of the ATLAS strip detector presented in figure 1a after a red laser scan across three strips for varied values of interface charge density Q_f . The bias voltage during the charge collection was 300 V while the laser diameter was $10\text{ }\mu\text{m}$. The strip implant edges are marked by dashed black lines. The charges are normalized to the maximum charge collected at $Q_f = 1 \times 10^{10}\text{ cm}^{-2}$.

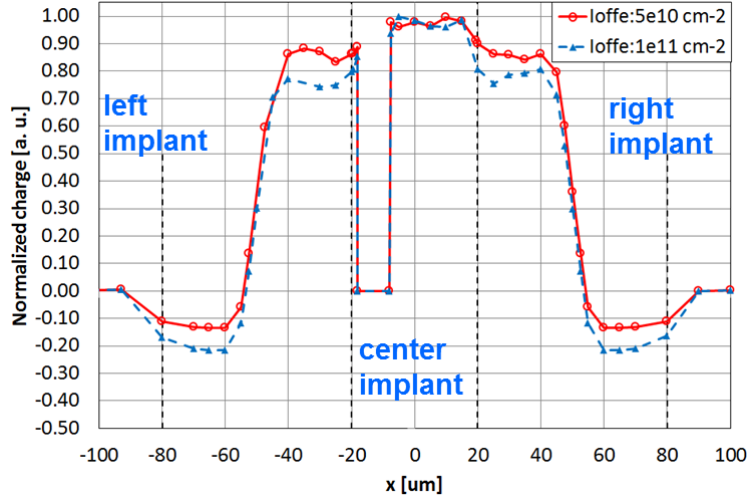


Figure 3: Charges collected at the centermost strip of the Ioffe Institute-design strip detector presented in figure 1b after a red laser scan across three strips for two values of interface charge density Q_f . The charge collection was done at $V = 400\text{ V}$ while the laser diameter was $10\text{ }\mu\text{m}$. The strip implant edges are marked by dashed black lines. The charges are normalized to the maximum charge collected at $Q_f = 5 \times 10^{10}\text{ cm}^{-2}$.

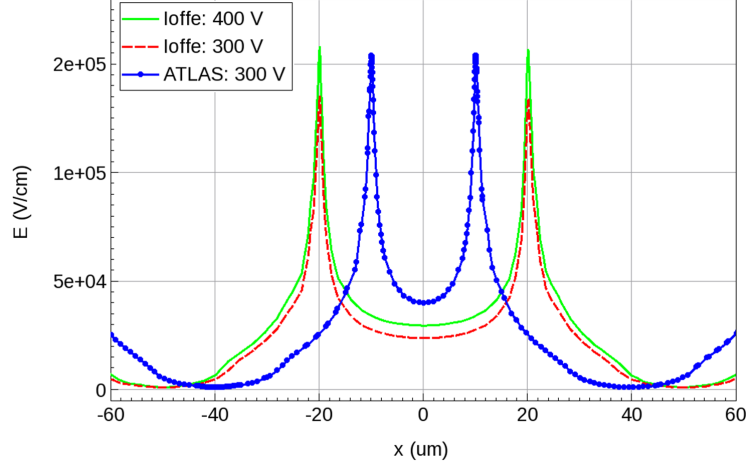


Figure 4: Electric field distributions parallel to the detector surface at $0.8 \mu\text{m}$ depth for the two detector designs with $Q_f = 1 \times 10^{11} \text{ cm}^{-2}$. Voltages used for charge collection in both detectors are included, as well as $V = 300 \text{ V}$ for the Ioffe Institute detector for clearer comparison with the ATLAS detector.

amount of charge before the edges of the interstrip gap. Finally, it can be observed from figure 5 that the effect of reversed polarity signals for laser positions beyond midgap from the readout strip is still present also for the lowest value of Q_f .

The laser scan results, with decreased laser diameter, of the Ioffe Institute-design strip sensor in figure 6 also display new features in charge collection behavior with respect to figure 3. The negative polarity signals in figure 6a between adjacent and centermost strips at around $x = |70| \mu\text{m}$ are now increased by about 17% and 12.5% for Q_f values $5 \times 10^{10} \text{ cm}^{-2}$ and $1 \times 10^{11} \text{ cm}^{-2}$, respectively. As for the ATLAS-design, the polarity reversal at midgap is significantly more abrupt than in figure 3, taking place within $5 \mu\text{m}$.

The amplitudes of the positive signals collected in the area of the oxide, with laser distance from the readout strip less than midgap, are also considerably lower, moving from about 70% to 60% with increased values of Q_f . Notably for both values of Q_f , the positive signal collected at oxide reaches a local maximum close to midgap, immediately before polarity reversal.

The charge collection plots in figure 6a at the centermost strip have a Q_f dependence when the laser spot is getting closer to the right edge of the implant, free of metallization. To further investigate the Q_f dependence when the laser spot is over the strip implant, the scans at the readout strip were repeated without any metallization. The results in figure 6b show that the charge collection of lower Q_f fluctuates within 10% with no descending pattern towards and beyond the implant edge. However, the curve for higher Q_f has

a descending shape towards the implant edge with 20% lower charge collected at the edge than the charge collected at lower value of Q_f . The charge collection of the two Q_f values essentially converges within 10 μm from the implant edge towards its center. Thus, for 1 μm red laser diameter the differences in Q_f at the interstrip gap also affect the charge collection of a charge injection done over the implant (with strip metallization removed) up to few microns from the implant edge.

Rather than having linear or smoothed extension of collected charge from the center of the implant towards the implant edge, the curves display a ramped or sawtooth behavior. The small dip at implant center could be interpreted as a result of local electric field minimum, seen in figure 4, leading to decreased charge collection. The second small dip at $x = |10| \mu\text{m}$ cannot be explained by physical processes and the surrounding datapoints linearly decreasing towards implant edge (for lower Q_f) support the interpretation that the fluctuation of the collected charge is a simulation artifact in the high concentration and high field region where calculation of transient currents is more demanding. Since this does not change the overall trends of charge collection at different surface regions of the strip sensor, the further investigation of the fluctuation is left to a later study.

Since the silicon sensors at the LHC-experiments are typically AC-coupled, a strip sensor configuration with AC-coupled strips was also investigated. The essentially identical charge collection results between DC- and AC-coupled sensors after simulated red laser scans displayed a coupling independent behavior.

3.2.1. Critical interface charge density

The strong dependence of the reversed polarity signals, collected beyond midgap from the readout strip, on Si-SiO₂ interface charge density Q_f is seen clearly in the plots of sections 3.1 and 3.2. This poses a question, is it possible to find a threshold level of Q_f beyond which the effect of negative polarity signals vanishes.

The iteration of Q_f values from $5 \times 10^{10} \text{ cm}^{-2}$ to $0.7 \times 10^{10} \text{ cm}^{-2}$, for laser scans of a Ioffe Institute-design sensor in the region of the interstrip gap where negative polarity signals appear, is presented in figure 7. As can be seen, the negative charge collected at the centermost strip has a strong dependence on Q_f and moves towards zero with decreased Q_f values. When the collected charges at $x = -60 \mu\text{m}$, where their amplitude is at maximum in figure 7, are plotted as a function of Q_f in figure 8, three regions are observed. First, a region where negative signals settle to zero at $Q_f \leq 0.8 \times 10^{10} \text{ cm}^{-2}$, then a strongly dynamic region of negative signal increase at $0.8 \times 10^{10} \text{ cm}^{-2} < Q_f < 2 \times 10^{10} \text{ cm}^{-2}$, and ultimately a region close to a plateau for higher values of Q_f .

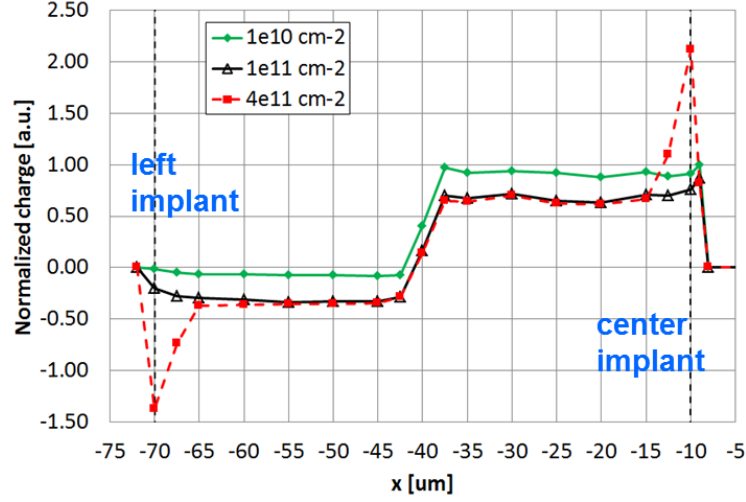


Figure 5: Corresponding red laser scan to figure 2 with laser diameter decreased to $1 \mu\text{m}$. Due to identical charge collection on both sides of the centermost strip, only left and center strips are plotted. Charges are normalized to the maximum collection at $Q_f = 1 \times 10^{10} \text{ cm}^{-2}$.

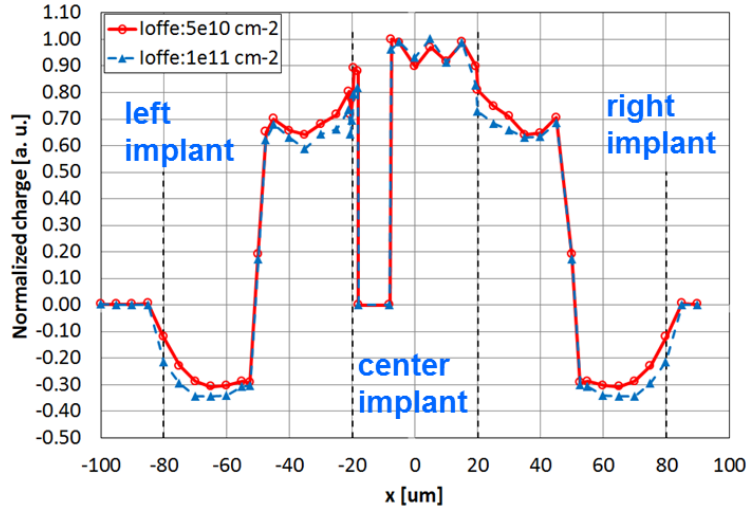
Thus, the negative polarity signals display an exclusive dependence on Si-SiO₂ interface charge states for a short range charge injection from the strip side at a given voltage and bulk doping.

3.3. Interstrip scans from the backplane

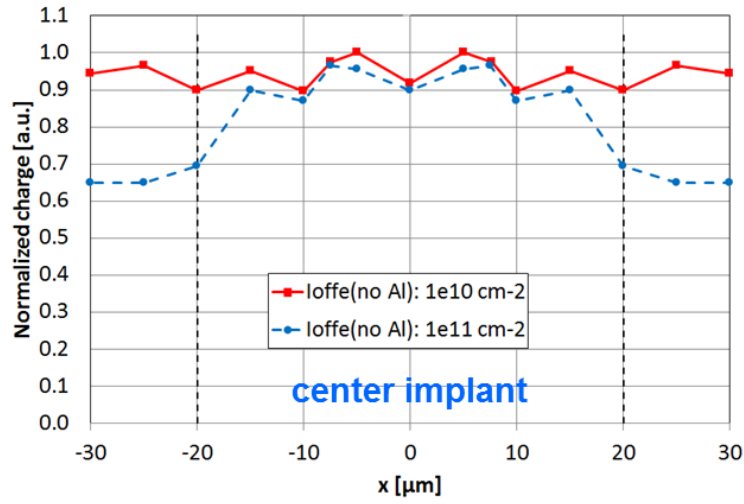
The red laser scans of the unsegmented n⁺-side of a Ioffe Institute-design strip sensor were enabled by removing the metallization from the backplane of the modelled structure. The absence of the reversed polarity signals observed in earlier measurements [5] is reproduced by the simulation, as seen in figure 9. No dependence on Q_f is observed when the laser is moving below interstrip gap.

However, when approaching the readout strip at the center of the modelled sensor structure, the $1 \mu\text{m}$ diameter laser displays features in the transient signals induced from the hole drift (as opposed to the electron drift from front surface injection), not seen in the measurement. The highest charge is now collected when the laser spot is below the oxide, some $5 \mu\text{m}$ from the readout strip. Then a 10% drop in the collected charge is observed at the implant edge and at the implant center.

When the backplane scan is repeated with a $10 \mu\text{m}$ diameter laser that matches the experimental diameter, shown in figure 9, no drop at the implant edge is observed and the measured behavior is reproduced closely. As in measurement [5], when the $10 \mu\text{m}$ diameter laser is moved above the interstrip gap the charges collected at the centermost strip never go to zero. This is opposite to the charge collection results of $1 \mu\text{m}$ diameter



(a) Illumination with 1 μm diameter red laser.



(b) Al removed.

Figure 6: (6a) Corresponding red laser scan to figure 3 with laser diameter decreased to 1 μm . (6b) Red laser scan across the centermost strip implant when the strip metallization has been completely removed. Collected charges are normalized to the maximum collection at the lower value of Q_f in each figure.

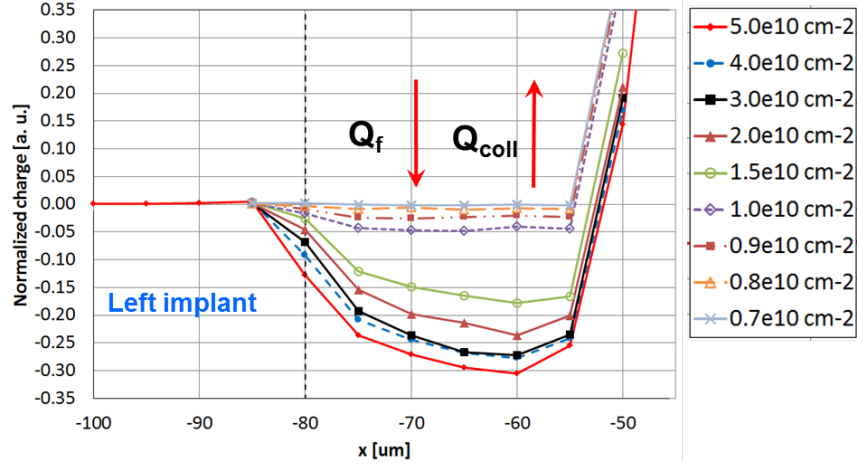


Figure 7: Red laser scans for a threshold Q_f where negative polarity signal vanishes. The detector and laser parameters are as in figure 6a. The collecting contact at $-20 \mu\text{m}$ (centermost strip) is not pictured. The red arrows indicate the dependence of the collected charge (Q_{coll}) on the interface charge density (Q_f).

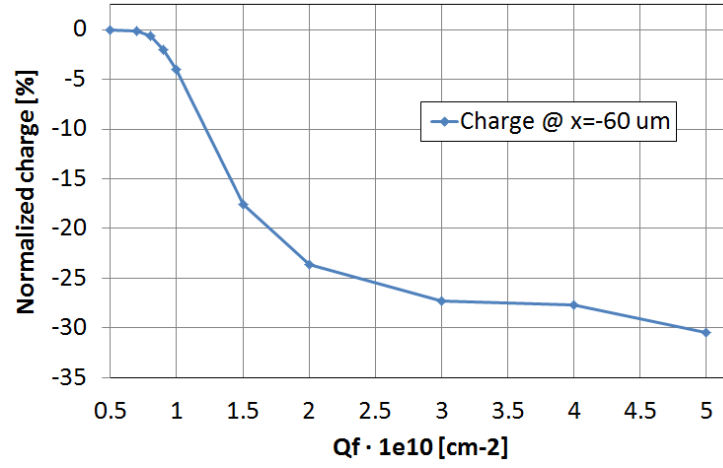


Figure 8: Corresponding evolution of collected charge with Q_f to figure 7 with cut made at $x = -60 \mu\text{m}$. The negative polarity signal vanishes when $Q_f \leq 0.8 \times 10^{10} \text{ cm}^{-2}$.

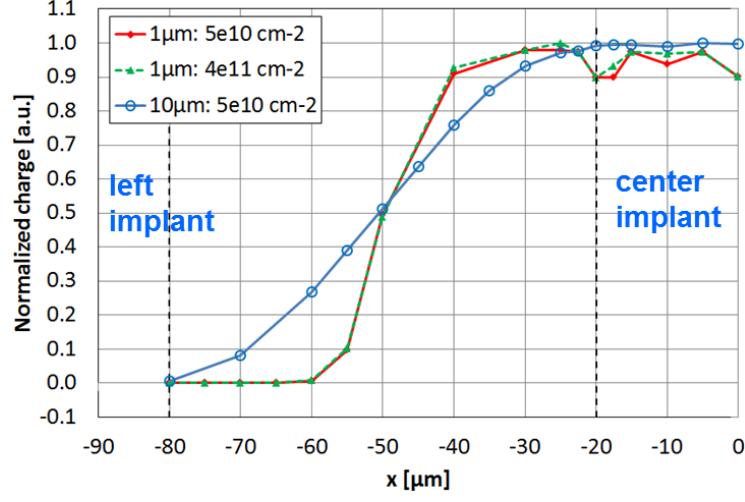


Figure 9: Charges collected at the centermost strip of the Ioffe Institute strip detector after a red laser scan from the backplane (n^+ -side) for two values of interface charge density Q_f . The charge collection was done at $V = 400$ V while the laser diameter was varied from 1 to 10 μm . The strip implant edges are marked by dashed black lines. Collected charges are normalized separately for the two laser diameters to enable comparison.

laser, as can be seen from figure 9. Thus, the spatial spread of the red laser is in important role in the shaping of charge collection distribution between and across the strips.

To further investigate the dependencies of the charge collection behavior after 1 μm diameter laser backplane illumination in the vicinity of the readout strip, the laser position was fixed to the implant edge ($x = -20$ μm in figure 9) and charge collection was monitored as a function of Q_f , as shown in figure 10. As can be seen, for comparison the charge injection was also repeated from the strip-side. The Q_f range was set to include values below and above the experimentally observed value $Q_f = 5 \times 10^{10} \text{ cm}^{-2}$ [6].

When laser is at the strip-side in figure 10, a clear charge multiplication (CM) effect is seen at $Q_f > 3 \times 10^{11} \text{ cm}^{-2}$. At values below this, increased Q_f results in significantly decreased positive collected charges due to increasing negative contribution from electron drift along the surface of the interstrip gap. The increase of Q_f increases also the electric field peaks at the implant edges. After the threshold value mentioned above this leads to CM of charge carriers that with further increase of Q_f fully compensate for the decreased collected charge. However, when charge injection is done from backplane, the collected charge is completely independent from Q_f and no CM is seen. Thus, effects from these parameters cannot explain the 10% drop in the collected charge at the implant edge in figure 9.

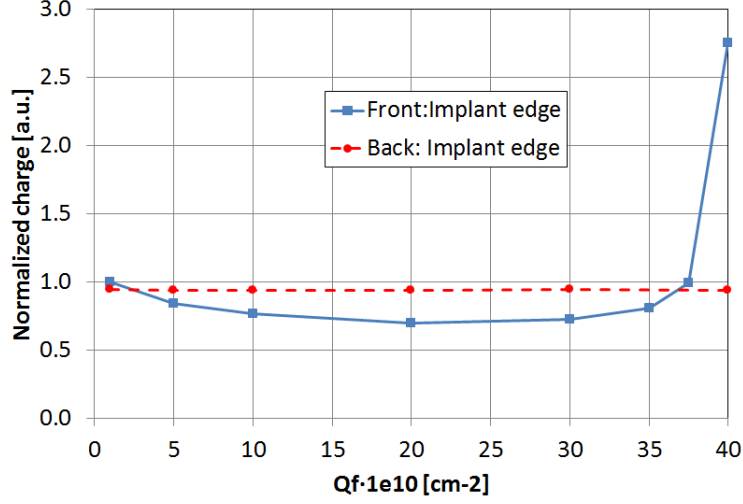


Figure 10: Charges collected after red laser illumination both from strip-side and backplane at the implant edge of the collecting contact of the Ioffe Institute strip detector. The collected charges are normalized to the charge collected at the lowest value ($1 \times 10^{10} \text{ cm}^{-2}$) of interface charge density Q_f from strip-side charge injection. The charge collection was done at $V = 400 \text{ V}$ while the laser diameter was $1 \mu\text{m}$.

3.4. Transient signals

To investigate the time evolution of the transient signals induced by the red laser, two laser spot positions were considered, $5 \mu\text{m}$ from the readout strip and $5 \mu\text{m}$ from its adjacent strip. These positions enable the study of transient currents leading to both positive and negative collected charges in the case of short range charge injection from the strip-side. Since the current response is

$$i(t) = \frac{d}{dt} Q_{\text{coll}}(t), \quad (1)$$

the features of the collected charge distribution as a function of position, presented in the previous sections, can also be seen in the transient current plots.

The current pulses in a red laser illuminated Ioffe Institute-design strip sensor at $V = 400 \text{ V}$ in figure 11 show that the duration of the negative current response is identical to the width of the positive current response. Also distinct is the smaller amplitude of the negative current pulse when $t < 2 \text{ ns}$. Both pulses induced by the electron drift have identical low-amplitude positive tail that goes to zero at about 5 ns . As can be seen from the time integrals of the transient currents, i.e. induced charges, this results in the reduction of the negative charge until the charge collection is complete.

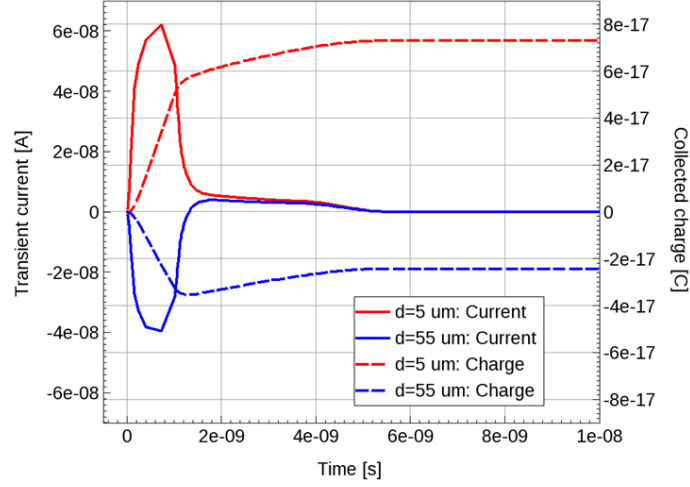


Figure 11: Transient current signals and collected charges after red laser illuminations. Two laser positions are considered, $5 \mu\text{m}$ and $55 \mu\text{m}$ from the collecting contact when the interstrip gap is $60 \mu\text{m}$. The interface charge density was $Q_f = 4 \times 10^{11} \text{ cm}^{-2}$.

4. Discussion

To provide an interpretation of the observed results in this study, it is considered that when the readout contact is a cathode, as in p-on-n strip sensors, holes drifting towards it and electrons drifting away from it induce a positive transient current that accumulates a positive collected charge. Reversed directions result in reversed polarity charge signals.

These statements are just consequences of the Ramo's theorem [16, 17], which gives an accurate result for the induced current, that is the charge induction rate, as

$$i = -qE^*v = \frac{dQ}{dt}, \quad (2)$$

where $q = \pm e$ is the carrier charge with e as the elementary charge, E^* is the weighting electric field and v is the charge drift velocity.

1. The 10-fold reduction of the laser diameter from the experimentally used value [5, 6] to $1 \mu\text{m}$ in figures 2 and 5 for ATLAS-design as well as in figures 3, 6a and 9 for Ioffe Institute-design, resulted in several distinct effects. First, when the laser spot position was moved across the interstrip oxide, a decrease in the positive collected charge and an increase in the absolute value of the negative polarity charge was observed. This can be seen as the result of the smaller spatial distribution of the charge carrier generation that leads to 10 times smaller averaging of the effects to the carrier transport from

the electric field distribution and drift distances parallel to the sensor surface. For the same reason the polarity reversal at the midgap moves closer to a step function, seen clearly in figures 5 and 6a. The same feature is observed at the edge of the strip implant. Thus, the CCE reduction and the sharpness of its changes are defined by the size of the beam.

2. The effects of smaller diameter laser spot also include a visible reduction of the Q_f dependence, i.e. the charges collected from laser illumination over the interstrip oxide have decreasing differences with increased Q_f . Evidence from figures 2, 5 and 8 indicates that for the smaller diameter charge injection there is an upper threshold value of Q_f beyond which only limited increase in negative polarity signals is seen with increased Q_f in the lower field regions of the interstrip gap.
3. In figure 6b the increased resolution of the laser displays the Q_f dependence of the collected charge when the laser spot is moved over the readout strip implant close to its edge when the strip metallization has been removed. The order of magnitude difference in Q_f for the two curves results in about 20% lower collected charge for the higher Q_f at the edge of the strip implant while the Q_f dependence essentially vanishes when the 1 μm diameter laser spot is moved 10 μm from the implant edge towards its center.

It should be emphasized that the losses of the laser light in the p^+ implant do not exceed 10% which is significantly less than the drop of about 30% of CCE for the two higher Q_f values in figure 6 when the laser spot is moved to the edge of the collecting strip implant and over the interstrip oxide.

4. The interpretation of earlier experimental observations concluded that the oxide layer with the attractive electric field may be considered as a "sink" for electrons that are moving close to the surface with the probability to reach the surface and be trapped in the interstrip gap significantly higher than for those, which are generated under the p^+ implant [6]. Since substantial reduction of the collected charge is observed at laser positions less than midgap distance from the collecting strip, the total transient current signal can be considered as a composite of the currents induced by the carrier drifts along the surface (I_{surf}) and orthogonal to the surface through the sensor thickness (I_{signal}) as

$$I_{\text{tot}} = I_{\text{signal}} + I_{\text{surf}}. \quad (3)$$

These are illustrated in figure 12a. With the statements from the first paragraph of this section and (3) the curves in figure 6b can now be interpreted of having minimal contribution from the opposite sign I_{surf} to I_{tot} in the middle of the p^+ implant, while its share increases when the point of charge injection moves to the implant edge, i.e. when the electron drift along the surface of the interstrip gap changes

from negligible to significant.

If I_{surf} is broken into two components with opposite velocity vectors, as in figure 12a, the increase in collected charges close to midgap in figures 5 and 6a can be interpreted to be the result of the components compensating each other with close to equal amplitudes. As a result, in the middle of the interstrip gap I_{tot} has decreased contribution from I_{surf} . When the position of charge injection moves closer to the implant edge of the collecting contact, the two opposite components of I_{surf} become increasingly non-equal, leading to growing opposite sign contribution to I_{tot} .

5. To understand the 10% decrease in collected charge after red laser illumination from the sensor backplane at a position opposite to the implant edge of the collecting strip in figure 9, the investigation presented in figure 10 revealed the effect to be Q_f independent, i.e. the holes drifting through the sensor bulk are not interacting with the layer of accumulated electrons in the interstrip gap. Thus, the positive I_{signal} induced by the hole drift towards the cathode strip is then the sole component of I_{tot} . In addition, the datapoint at the implant edge does not constitute any descending or ascending trend in the charge collection curves and when the backplane scan is repeated with a $10\ \mu\text{m}$ diameter red laser the effect vanishes. Hence, the lower collected charge at the implant edge is not regarded as a physical effect but a simulation artifact as the few percent fluctuations in figure 6b.
6. The strip-side red laser illuminations at the implant edge of the collecting strip in figure 10 show strong dependence on Q_f . Due to the charge injection position, the only possible direction for I_{surf} is away from the collecting strip. Thus, even though both I_{surf} and I_{signal} are now induced from the drift away from the collecting contact, I_{surf} towards the adjacent strip and I_{signal} towards backplane, they clearly induce opposite polarity signals. Hence, as in the above interpretation of compensation of the two components of I_{surf} , the equal sign charge carriers with different direction velocity vectors compensate each other.
7. Following the model proposed in [6] the curvature of the electric field under SiO_2 in interstrip gap has a minimal potential for electrons at the interface and the saddle point with maximal electric field at certain distance in the bulk. Such a potential distribution can act as sink for the electrons. Undoubtedly the local potential maximum seen in figures 12a and 12b works against the drift of electron cloud to the interface, however, some fraction of the cloud can diffuse towards the interface via the potential maximum. Obviously the shape of the peak is important for the charge losses and the shape changes with Q_f , as can be seen from figure 12b.

The influence of sinks to the charge collection can also be concluded from figure 11. The transient

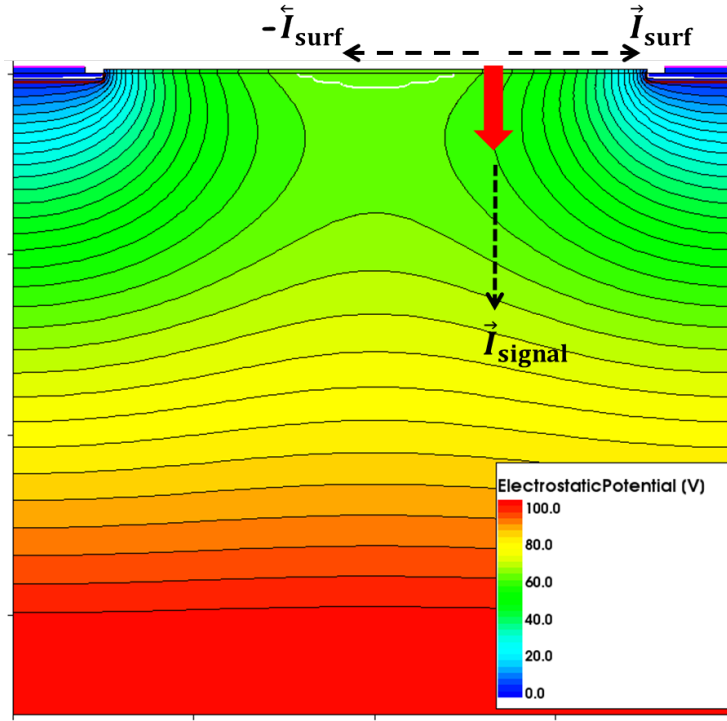
current curve for $d = 55 \mu\text{m}$ ($5 \mu\text{m}$ from the strip adjacent to the readout strip) displays first a higher amplitude negative polarity signal due to electron drift from the high electric field region, repulsed by the injected electrons, towards the readout strip. Then a low amplitude positive 'tail' is induced due to the drift of the electrons, not trapped at the potential minimum, away from the readout strip towards the sensor backplane. Identical 'tail' is observed for $d = 5 \mu\text{m}$ transient curve in figure 11, showing that the accumulation layer electrons are again repulsed to the potential minimum region providing the low amplitude, slow component to the positive transient signal.

8. As was shown in figures 7 and 8, it is possible to find values of Si-SiO₂ interface charge density Q_f within an order of magnitude of typical values seen in non-irradiated strip sensors that can reduce negative I_{surf} to insignificant level in a p-on-n strip sensor. In the particular cases of ATLAS and alternative Ioffe Institute topologies with different strip pitches and strip implant widths the values are in the range of $(0.8 - 1.5) \times 10^{10} \text{ cm}^{-2}$.
9. The resulting observations lead to the conclusion, that a charge injection through Si-SiO₂ accumulation layer of a segmented p-on-n silicon sensor induces I_{surf} of which sign is always opposite relative to I_{signal} . The level of influence from I_{surf} to I_{tot} is governed by the trapping produced imbalance between its two opposing components induced by the drifts parallel and normal to the sensor surface.
In the absence of I_{signal} , i.e. at charge injection positions beyond midgap from the collecting strip, the reversed polarity of I_{surf} is due to electron drift towards the collecting cathode of the p-on-n strip sensor.

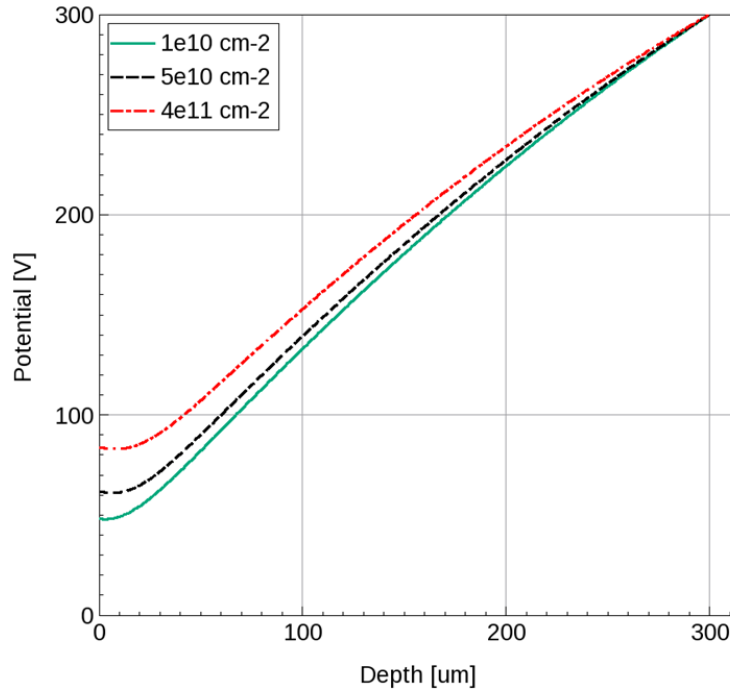
5. Conclusions

The performed simulations of the influence of Si-SiO₂ interface charge on the current response and charge collection efficiency reproduces all experimental features, i.e. negative fraction in the charge response and tens of percents reduction of CCE which were observed earlier [5, 6] in non-irradiated Si strip detectors. When agreement between measurement and simulation was obvious the simulations could be extended to parameter values beyond the experimental study with justified confidence on the results. The study demonstrated that:

1. Variation of the interface charge and its influence on the detector response in the performed modelling gives clear indication that the features are originated from the interface charge and defined by its density.



(a) Potential distribution in ATLAS strip sensor.



(b) Potential cut at midgap through sensor bulk.

Figure 12: Electrostatic potential distribution at $V = 300 \text{ V}$ up to $70 \mu\text{m}$ depth (12a) and the corresponding cut through the sensor bulk (12b) at the midgap between strips for varying values of Q_f in ATLAS strip sensor structure. (12a) also depicts an example of a charge injection by a red laser (red arrow) through the interstrip oxide layer and the resulting components of transient current.

2. There is a critical density of the interface charge which initiates the features and the value of critical density is not sensitive to the topology of the strip detector.
3. The critical interstrip charge density was defined and in the particular cases of ATLAS and alternative Ioffe Institute topologies, with different strip pitches and strip implant widths, the values are in the range of $(0.8 - 1.5) \times 10^{10} \text{ cm}^{-2}$.
4. Simulation of the charge collection in the interstrip gap with the laser beam spot equal to that used in the experiment ($10 \mu\text{m}$ diameter) or ten times less showed that the negative response in the active strip changes sharply its value in the middle of the interstrip gap. This shows a direct link to the trajectory of the collected charge cloud. It is important to which strip the electric field line and the related trajectory of the cloud flow in.

The performed study is a physical base for explanation and prediction of the influence of radiation on the detector performance. Generation of the charge at the Si-SiO₂ interface is a specific process sensitive to the properties of SiO₂ layer and its thickness. The results show the possibility for the irradiation effect stabilization and/or its minimization via optimization of interstrip gap passivation.

The results provide grounds to extend the study to the experimentally observed absence of reversed polarity signals in infra-red laser (with minimum ionizing particle-like carrier generation) illuminated strip sensors [5], as well as the possible sensitivity of n-on-p strip sensors to the effect, which is a strict plan for the nearest future.

References

- [1] D. Robinson, et al., Silicon microstrip detectors for the ATLAS SCT, Nucl. Instr. & Meth. A 485 (2002) 84–88. doi:10.1016/S0168-9002(02)00536-3.
- [2] L. Andricek, et al., Design and test of radiation hard p⁺n silicon strip detectors for the ATLAS SCT, Nucl. Instr. & Meth. A 439 (2000) 427–441. doi:10.1016/S0168-9002(99)00901-8.
- [3] P. P. Allport, et al., A comparison of the performance of irradiated p-in-n and n-in-n silicon microstrip detectors read out with fast binary electronics, Nucl. Instr. & Meth. A 450 (2000) 297–306. doi:10.1016/S0168-9002(00)00259-X.
- [4] H. W. Kraner, et al., Charge Collection in Silicon Strip Detectors, IEEE Trans. Nucl. Sci 30 (1983) 405–414. doi:10.1109/TNS.1983.4332300.

- [5] V. Eremin, J. Bohm, S. Roe, G. Ruggiero, P. Weilhammer, The charge collection in single side silicon microstrip detectors, Nucl. Instr. & Meth. A 500 (2003) 121–132. doi:10.1016/S0168-9002(03)00330-9.
- [6] E. Verbitskaya, et al., Effect of SiO₂ Passivating Layer in Segmented Silicon Planar Detectors on the Detector Response, IEEE Trans. Nucl. Sci 52 (2005) 1877–1881. doi:10.1109/TNS.2005.856907.
- [7] T. Peltola, Charge collection efficiency simulations of irradiated silicon strip detectors, JINST 9 (2014) C12010. doi:10.1088/1748-0221/9/12/C12010.
- [8] A. Bhardwaj, R. Dalal, R. Eber, T. Eichhorn, K. Lalwani, A. Messineo, T. Peltola, M. Printz, K. Ranjan, *Simulation of Silicon Devices for the CMS Phase II Tracker Upgrade*, Compact Muon Solenoid, CMS DN -2014/016 (2015).
- [9] T. Peltola, et al., A method to simulate the observed surface properties of proton irradiated silicon strip sensors, JINST 10 (2015) C04025. doi:10.1088/1748-0221/10/04/C04025.
- [10] T. Peltola, Simulation of radiation-induced defects, PoS 031 (2015) (VERTEX2015).
URL pos.sissa.it/archive/conferences/254/031/VERTEX2015_031.pdf
- [11] T. Peltola, et al., Characterization of thin p-on-p radiation detectors with active edges, Nucl. Instr. & Meth. A 813 (2016) 139–146. doi:10.1016/j.nima.2016.01.016.
- [12] R. Eber, Investigations of new sensor designs and development of an effective radiation damage model for the simulation of highly irradiated silicon particle detectors, Ph.D. thesis, Karlsruhe Institute of Technology (2013).
URL <http://ekp-invenio.physik.uni-karlsruhe.de/record/48328/files/EKP-2014-00012.pdf>
- [13] T. Peltola, Numerical simulations of semiconductor radiation detectors for high-energy physics and spectroscopy applications, Ph.D. thesis, University of Helsinki (2016).
URL <https://helda.helsinki.fi/bitstream/handle/10138/159441/numerica.pdf?sequence=1>
- [14] G. Ruggiero, Signal Generation in highly irradiated silicon microstrip detectors for the ATLAS experiment, Ph.D. thesis, Dept. Phys. Astr., University of Glasgow, Glasgow, U.K. (2003).

- [15] S. M. Sze, Physics of Semiconductor Devices, 2nd Edition, John Wiley & Sons, New Jersey, 1981.
- [16] G. Cavalleri, E. Gatti, G. Fabri, V. Svelto, Extension of Ramo's theorem as applied to induced charge in semiconductor detectors, Nucl. Instr. & Meth. A 92 (1971) 137–140. doi:10.1016/0029-554X(71)90235-7.
- [17] E. Gatti, G. Padovini, V. Radeka, Signal evaluation in multielectrode radiation detectors by means of a time dependent weighting vector, Nucl. Instr. & Meth. A 193 (1982) 651–653. doi:10.1016/0029-554X(82)90265-8.